Table of Contents

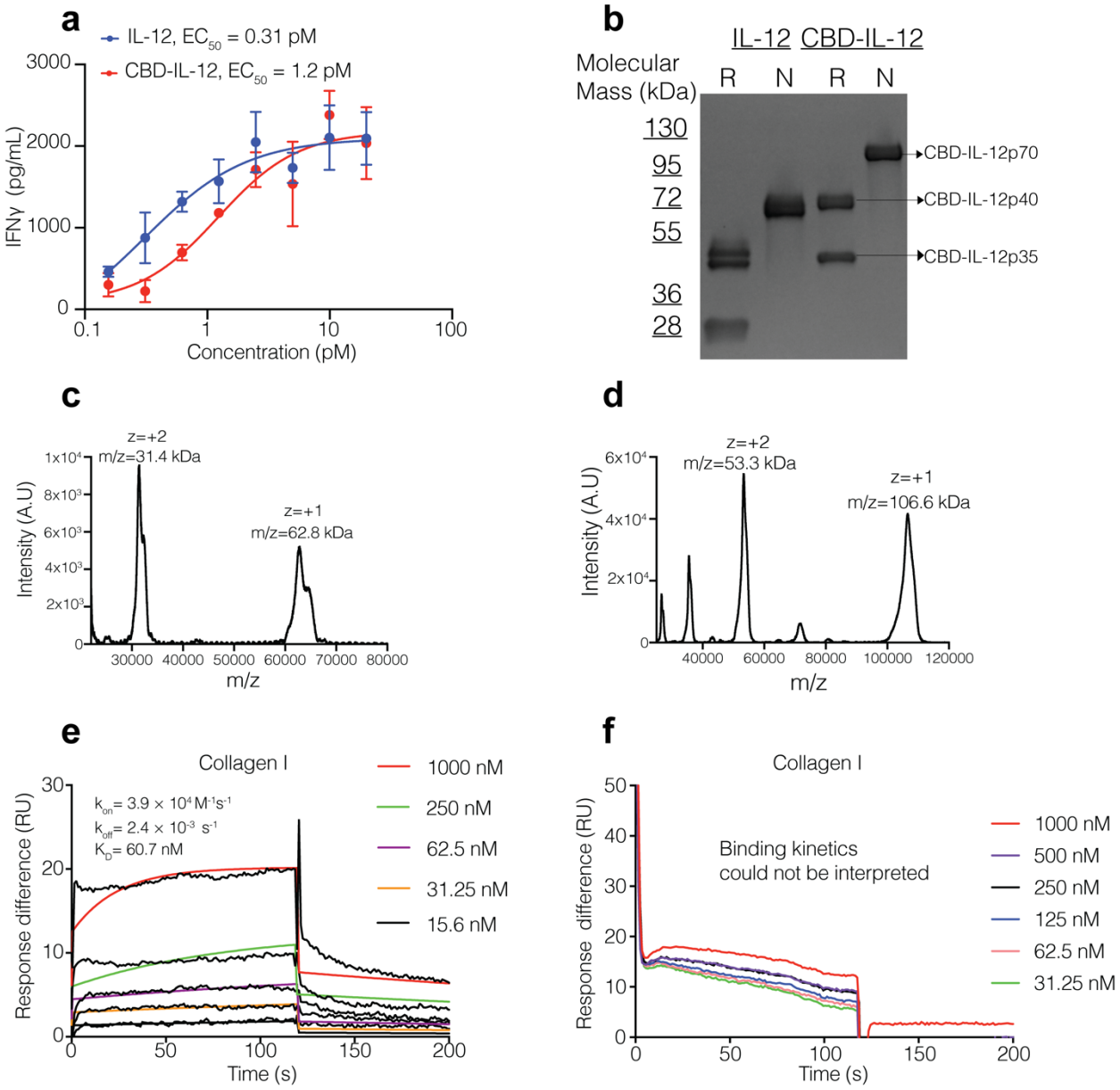

Supplementary Fig. 1 | Biophysical characterization of IL-12 and CBD-IL-12. a, Splenocytes were cultured in the presence of 10 ng/mL IL-2 and indicated amounts of IL-12 or CBD-IL-12 (n = 3). IFNγ in the supernatant was measured using ELISA. Data are mean ± SEM. **b,** SDS-PAGE for IL-12 and CBD-IL-12 under reducing (R) and non-reducing (N) conditions. As expected, two bands appear under reducing conditions for IL-12, corresponding to the p35 and p40 subunits. Under reducing conditions, these bands were shifted by ~20 kDa in the case for CBD-IL-12, indicating that one CBD molecule was fused to each subunit. **c,d,** MALDI-TOF linear positive mode spectra of IL-12 (**c**) and CBD-IL-12 (**d**). The single and double charged molecular ions are indicated for each molecule with a corresponding m/z value. **e,** SPR analysis of monoCBD-IL-12 (where CBD protein is only fused to the p40 subunit) binding to collagen I. **f,** SPR analysis of IL-12 binding to collagen I. Binding kinetics was not determined. All experiments were performed twice, with similar results.

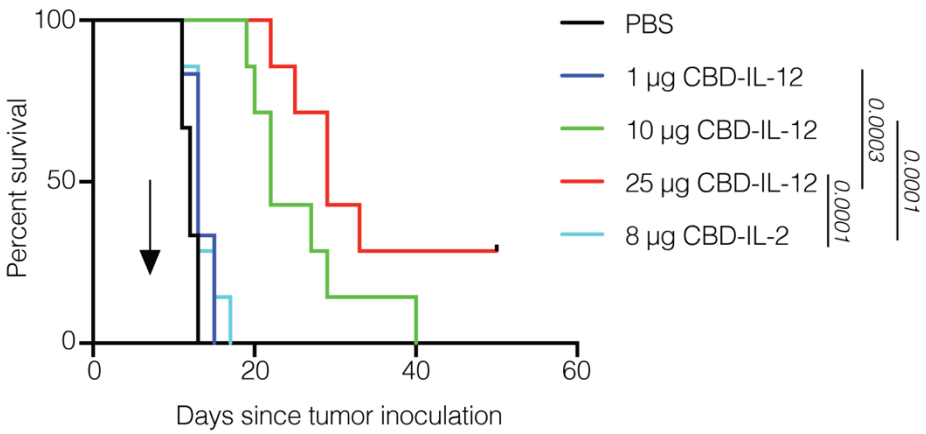

Supplementary Fig. 2 | CBD-IL-12 exhibits dose-dependent antitumor efficacy and is superior to equimolar CBD-IL-2. 5×10^5 B16F10 melanoma cells were inoculated intradermally on back skin and mice were treated with either PBS, CBD-IL-12 or CBD-IL-2 once on day 7 (n = 7 per group). 8 μg of CBD-IL-2 is equimolar to 25 μg of CBD-IL-12. Dose of CBD-IL-12 is based on IL-12 amount, i.e., 25 μg of CBD-IL-12 is equimolar to 25 μg of IL-12. Statistical analysis was done using log-rank (Mantel-Cox) test. Experiment was performed once.

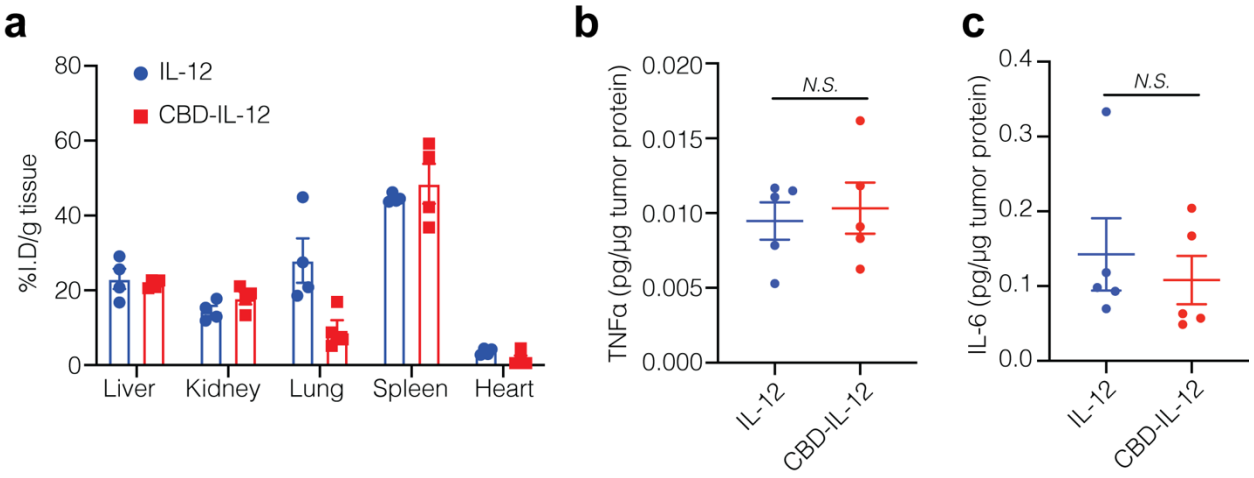

Supplementary Fig. 3 | IL-12 and CBD-IL-12 have similar biodistribution in tumor-free mice and induce similar levels of intratumoral TNFα and. IL-6. a, Balb/c mice were injected i.v. with 25 μg of DyLight 650-labeled IL-12 or CBD-IL-12 (n = 4 per group). Fluorescence intensity in each organ was measured using IVIS 1 hr post injection and normalized to the weight of the organ. Experiment was performed twice, with similar results. **b,c,** B16F10 melanoma-bearing mice were treated with either 25 μg IL-12 or equimolar CBD-IL-12 i.v. once on day 7 and tumors were harvested 4 days after treatment (n = 5 per group). Luminex assay was performed on tumor lysates and analyzed for indicated cytokines/chemokines. Cytokine levels were normalized by total protein content. Luminex analysis was performed once. Data are mean ± SEM.

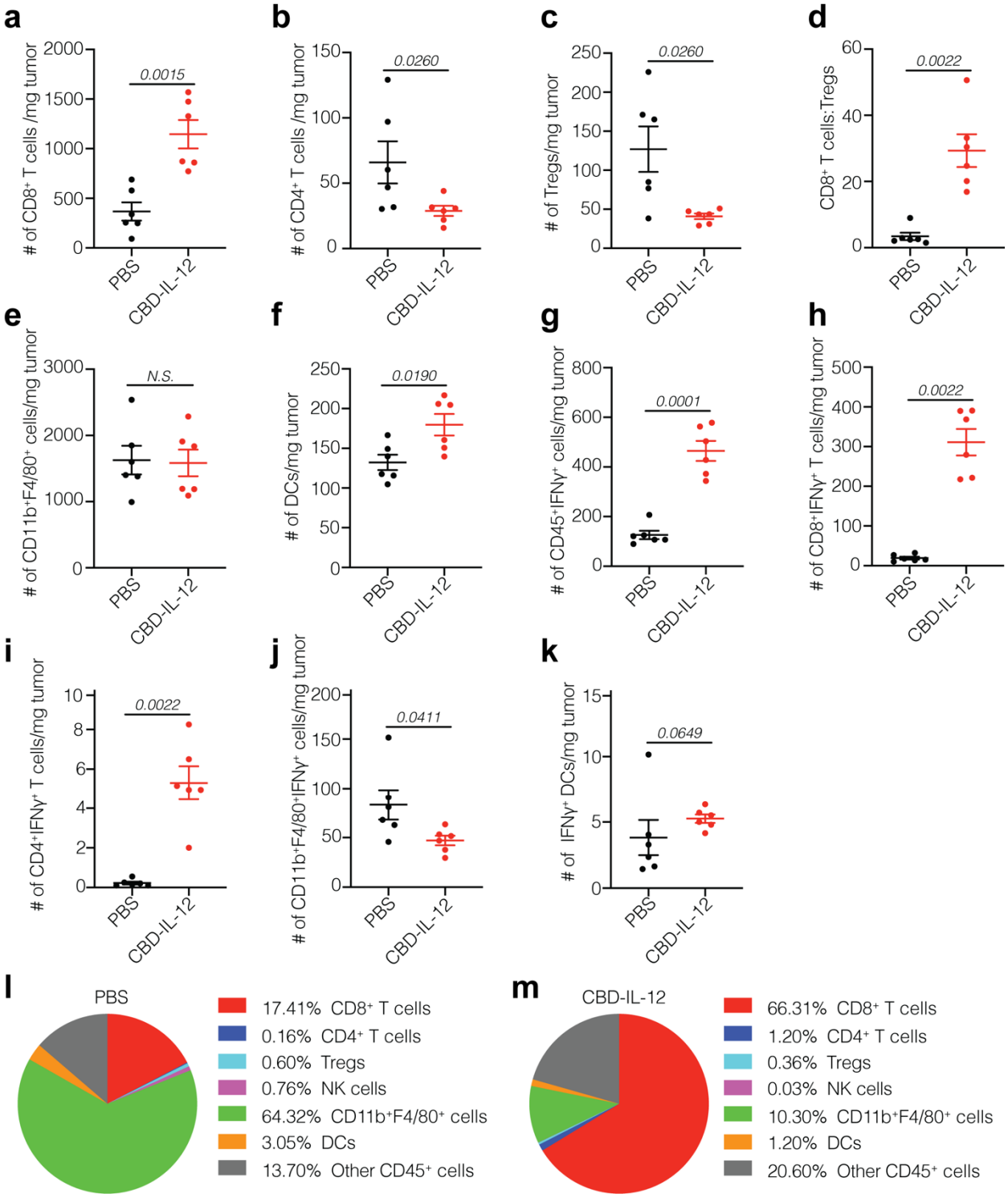

Supplementary Fig. 4 | CD8⁺ T cells in the tumor are major producers of IFNγ upon CBD-IL-12 therapy. a-m, 5×10^5 B16F10 melanoma cells were inoculated intradermally on back skin and mice were treated with either PBS or CBD-IL-12 once on day 6 (n = 6 per group). On day 10, 250 μg of brefeldin A (BFA) was injected i.p. and tumors were collected 5 hr post BFA injection. Tumors were processed and stained for flow cytometric analysis. Counts of $CD3^+CD8^+$ T cells (**a**), $CD3^+CD4^+$ T cells (**b**), $CD3^+CD4^+Foxp3^+$ Tregs (**c**) per mg of tumor. Ratio of $CD8^+$ T cells to Tregs (**d**). Counts of $CD11b^+F4/80^+$ cells (**e**) and $CD11c^+MHCII^+$ DCs (**f**) per mg tumor. **g-k,** Counts of $IFN\gamma^+CD45^+$ immune cells (**g**), $IFN\gamma^+CD8^+$ T cells (**h**), $IFN\gamma^+CD4^+$ T cells (**i**), $IFN\gamma^+CD11b^+F4/80^+$ cells (**j**) and $IFN\gamma^+$ DCs (**k**) per mg tumor. **l,m,** Pie chart representing percentages of $IFN\gamma^+$ cells within total $CD45^+$ cells after treatment with PBS (**l**) or CBD-IL-12 (**m**). Experiment was performed twice with similar results. Representative data are shown. Data are mean ± SEM. Statistical analyses were performed using unpaired, two-tailed t-test with Welch correction for **a,e,f,g** and a two-tailed Mann-Whitney test for **b,c,d,h,i,j,k** due to nonparametric data.

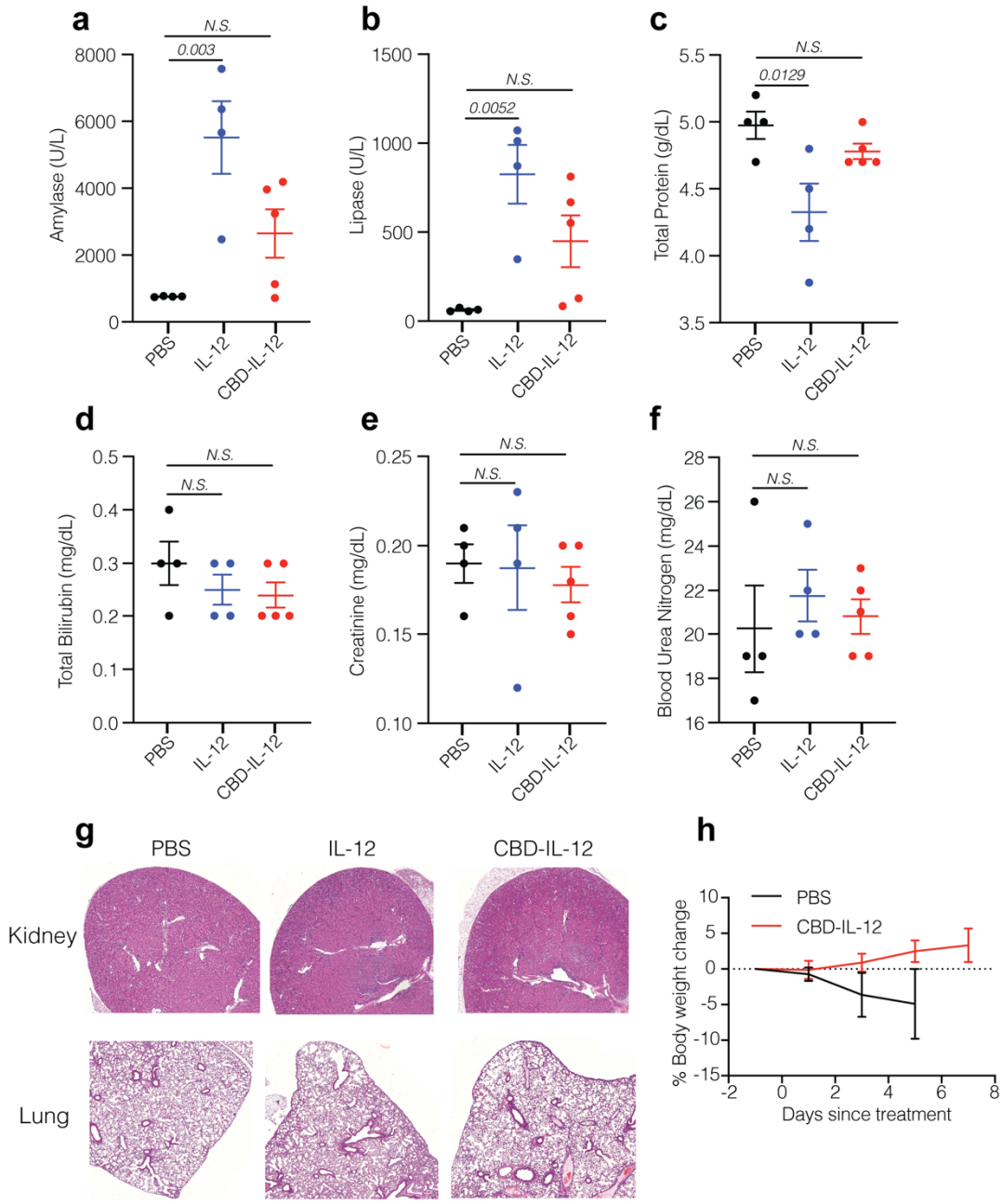

Supplementary Fig. 5 | CBD-IL-12 decreases pancreatic damage and does not cause lung and kidney damage. a-g, B16F10-tumor bearing mice received either PBS (n = 4), 25 µg IL-12 (n = 4) or 25 µg CBD-IL-12 (IL-12 molar eq., n = 5) via i.v. injection. **a-f,** 3 days after treatment, serum was collected and analyzed for indicated damage markers using Vet Axcel Clinical Chemistry Analyzer. Amylase (**a**) and lipase (**b**) indicate pancreas damage. Total protein (**c**) and total bilirubin (**d**) indicate liver damage. Creatinine (**e**) and blood urea nitrogen (**f**) indicate kidney damage. **g**, 3 days after treatment, kidneys and lungs from mice were harvested, fixed and stained with H&E. Representative images are shown. **h,** Body weight change of B16F10 melanoma-bearing mice treated with PBS (n = 5) or 25 µg CBD-IL-12 (IL-12 molar eq., n = 7) via i.v. injection. Lines represent mean ± SEM. Statistical analyses were done using ordinary one-way ANOVA with Dunnett's multiple comparison test. Experiments were performed twice with similar results.

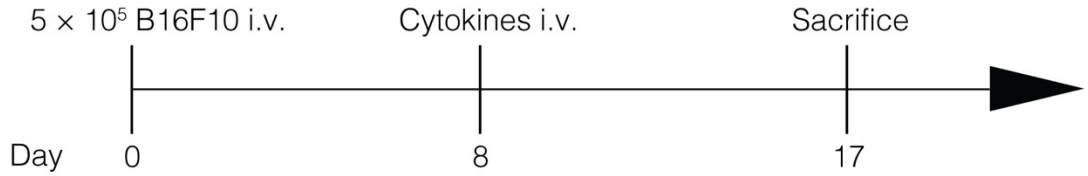

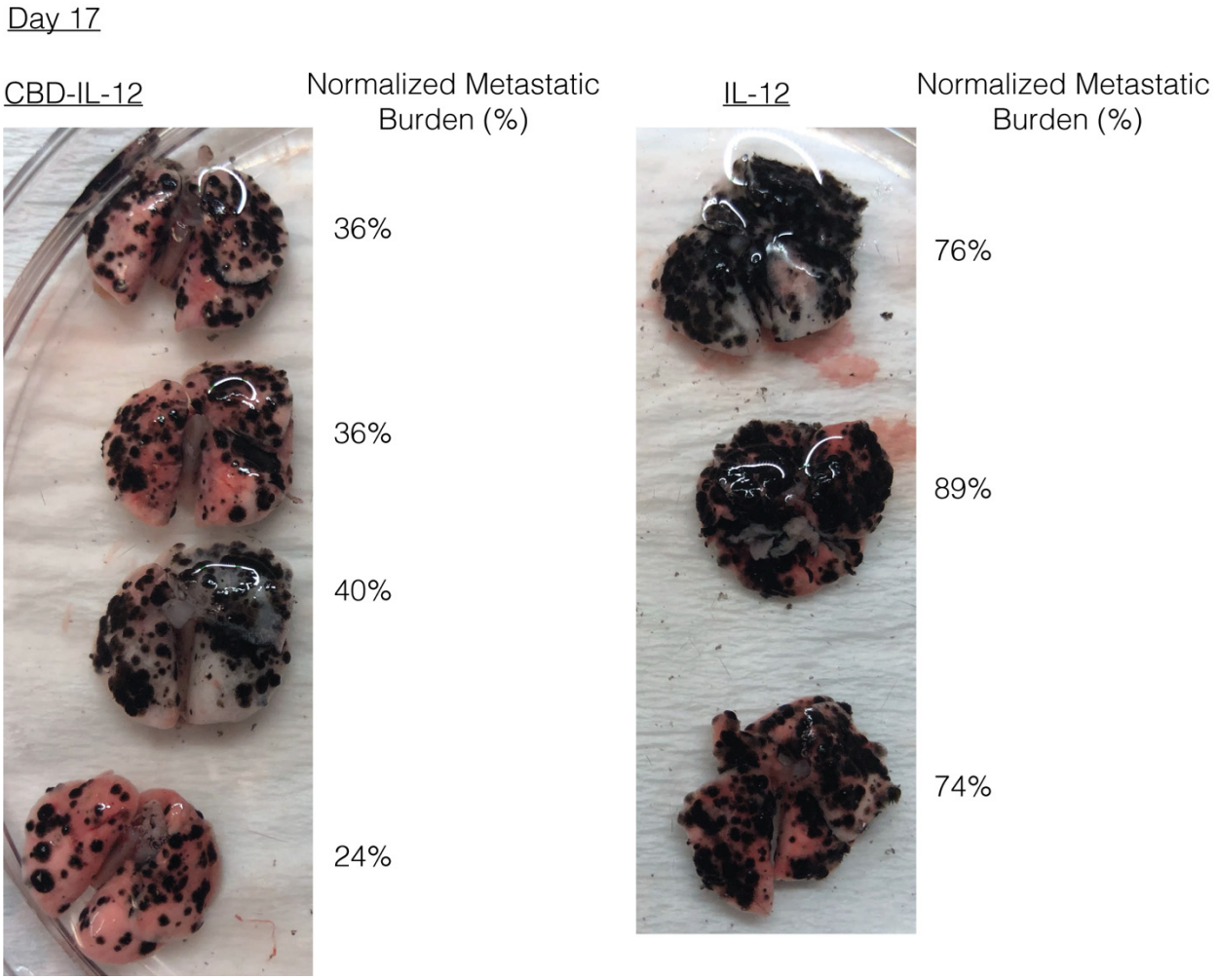

Supplementary Fig. 6 | CBD-IL-12 decreases metastatic burden in the lungs. 5 × 10^5 B16F10 cells were injected i.v. on day 0. 25 µg of IL-12. (n = 3) or equimolar CBD-IL-12 (n = 4) was administered 8 days after B16F10 inoculation, when metastatic nodules were visible. Data shown in Fig. 5a are depicted. Experiment was performed twice, with similar results.

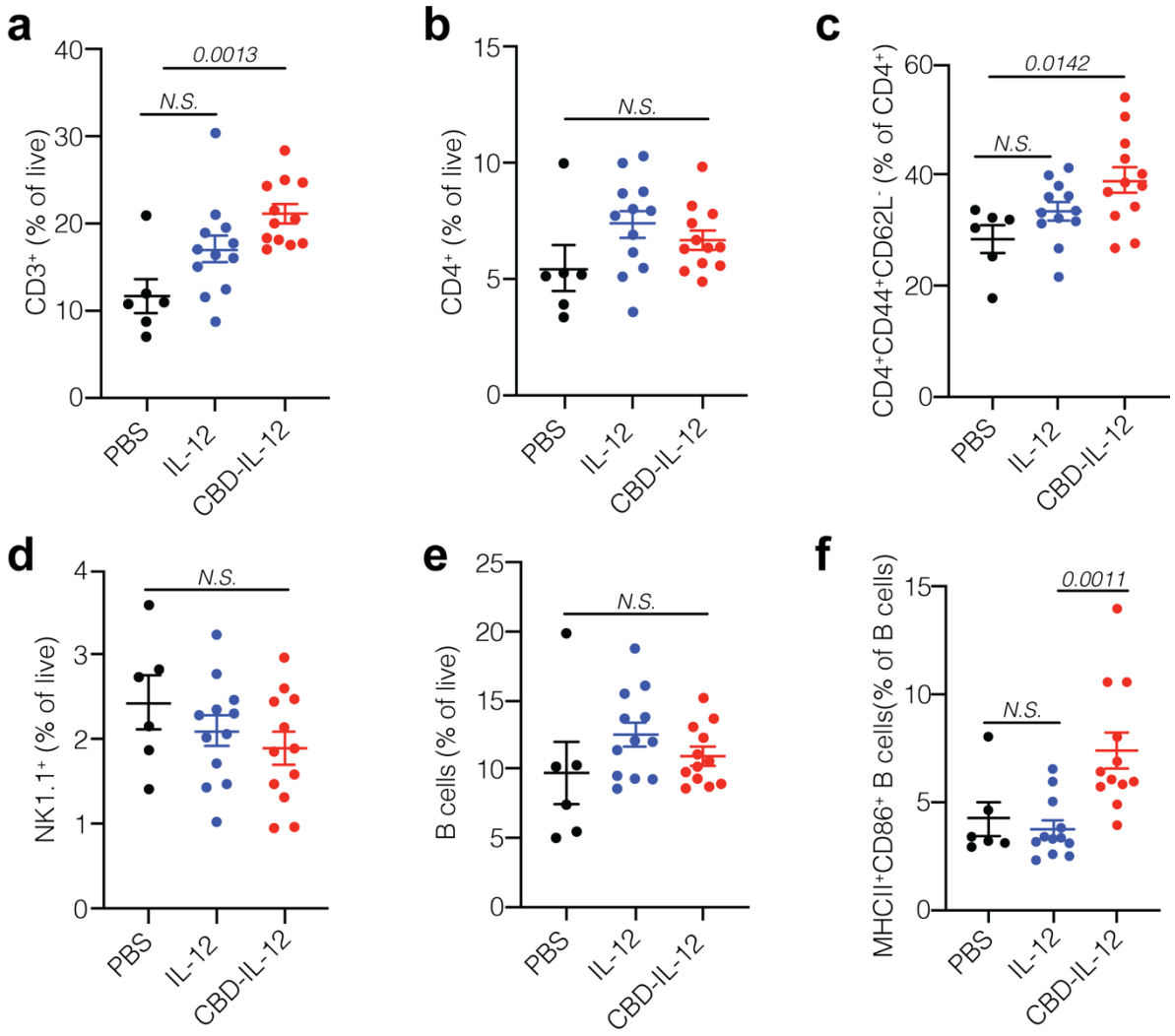

Supplementary Fig. 7 | Immune cell infiltration in the lungs of B16F10 metastases-bearing mice. a-f, 2.5 × 10^5 B16F10 cells were injected i.v. on day 0. Mice were treated with either PBS (n = 6), 25 µg IL-12 (n = 12) or with 25 µg CBD-IL-12 (IL-12 molar eq., n = 12) i.v. once on day 9 and lungs were collected on day 18. 2 × 10^6 live cells/well were plated for flow cytometric analysis. **a,** Percentages of $CD3^+$ T cells within live cells. **b,** Percentages of $CD4^+CD3^+$ T cells within live cells. **c,** Frequency of $CD3^+CD4^+CD44^+CD62L^-$ effector $CD4^+$ T cells within total $CD4^+$ T cells. **d,** Percentages of $NK1.1^+$ cells within live cells. **e,** Percentages of $CD45^+CD19^+$ cells within live cells. **f,** Frequency of $MHCII^+CD86^+$ B cells within total B cells (defined as $CD45^+CD19^+$). Lines represent mean ± SEM. Statistical analyses were done using ordinary one-way ANOVA with Tukey's test for parametric data. For nonparametric data (**f**), Kruskal-Wallis test followed by Dunn's multiple comparison was used. test

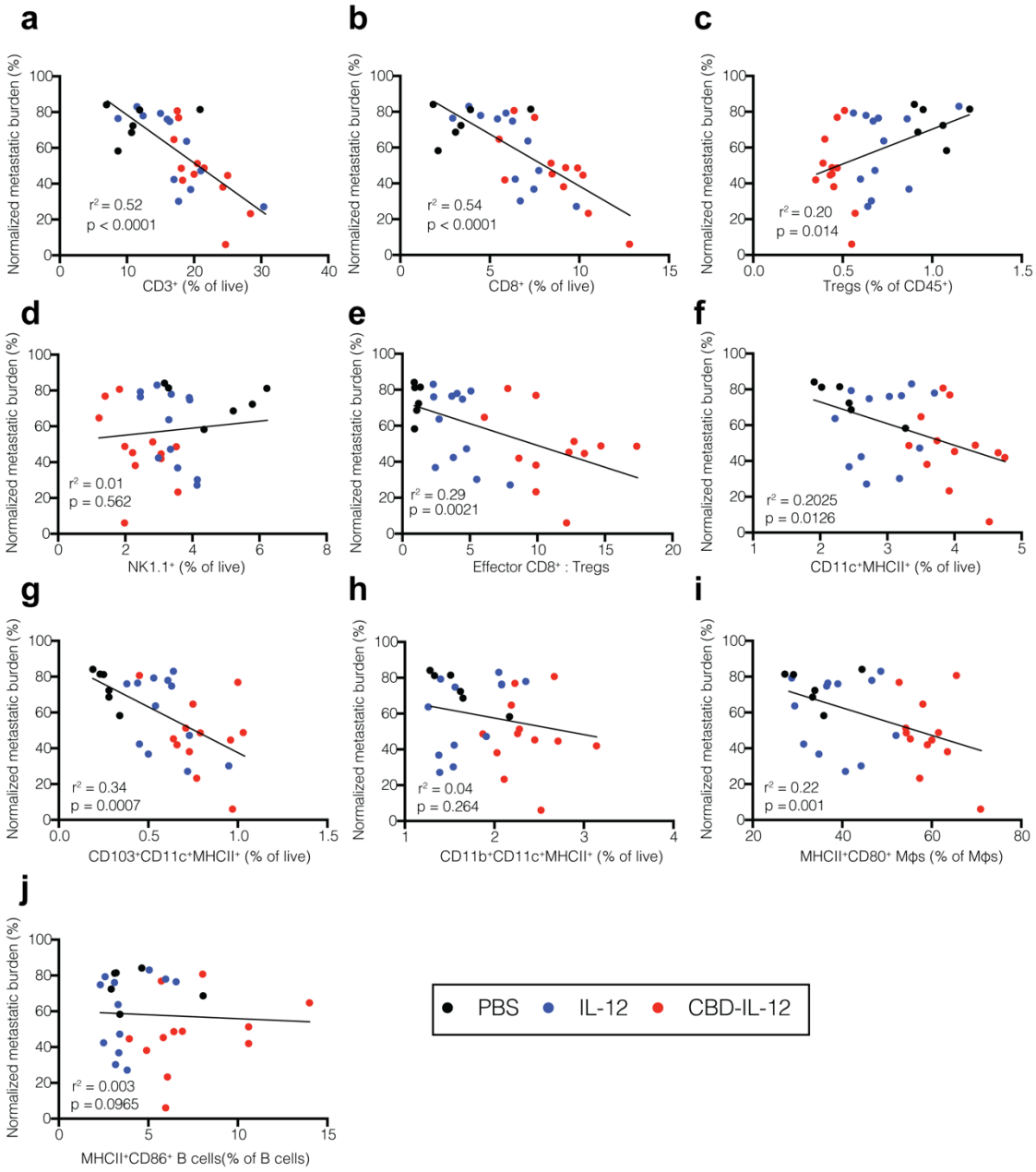

Supplementary Fig. 8 | Correlation analysis between various immune cell infiltrates and metastatic burden. a-j, Simple linear regression analysis was performed using data presented in Fig. 5b-i and Supplementary Fig. 7a-f. Mice were treated as described in Fig. 5b-i. PBS, n = 6. IL-12, n = 12. CBD-IL-12, n = 12. Metastatic burden was quantified using ImageJ software and normalized by the total area of the lung. Immune cell subsets are defined in Fig. 5 and in Supplementary Fig. 7.

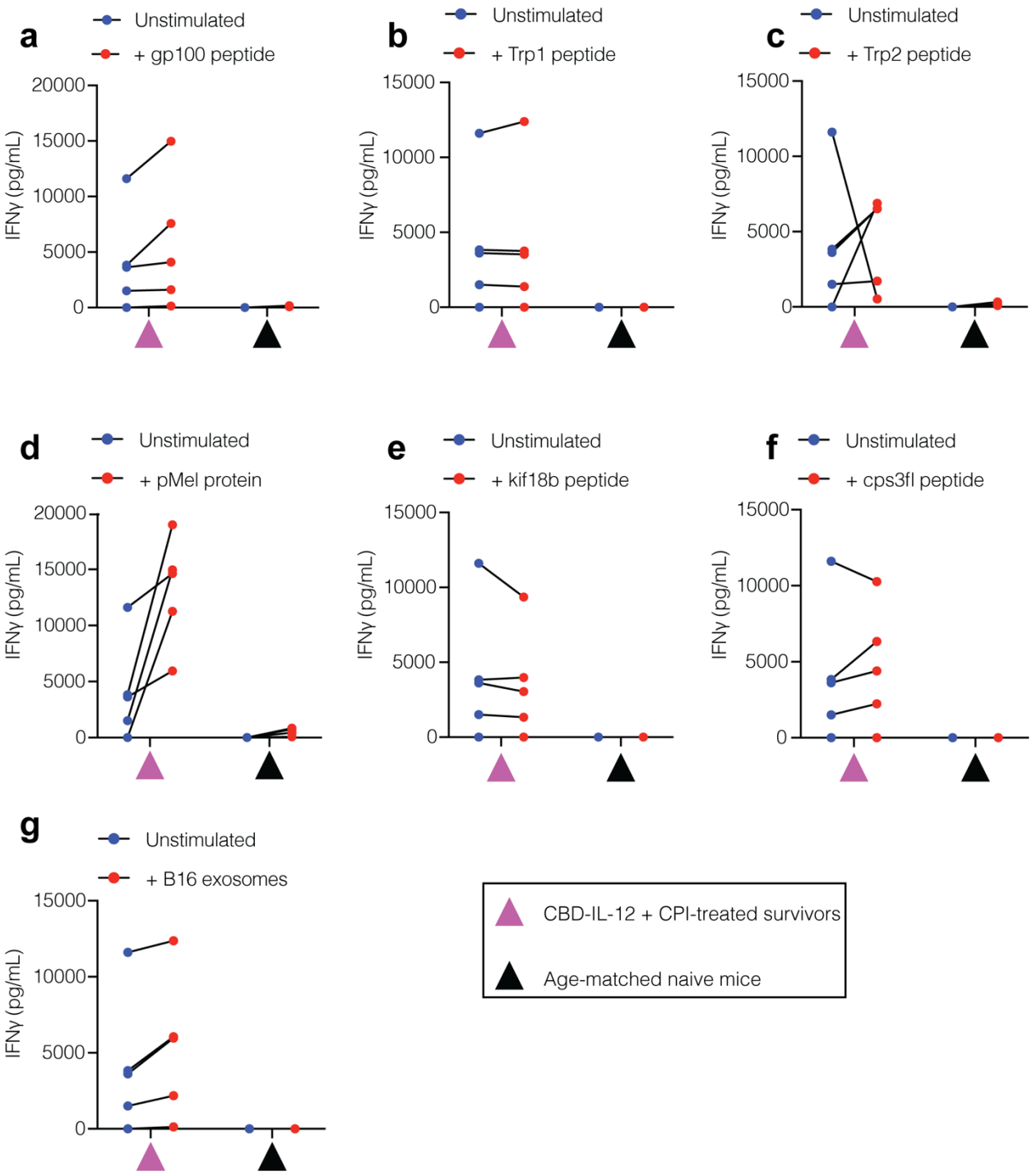

Supplementary Fig. 9 | IFNγ secretion of splenocytes from CBD-IL-12 + CPI-treated survivors and age-matched naïve mice upon antigen restimulation. a-g, Mice were treated as described in Fig. 6a,b. Spleens from surviving mice (n = 5) or age-matched naïve mice (n = 5) were harvested and stimulated with indicated antigens. IFNγ secretion from the supernatants was detected by ELISA. The differences between stimulated and unstimulated wells were used to construct the heat map shown in Fig. 6c. Experiment was performed twice, with similar results.

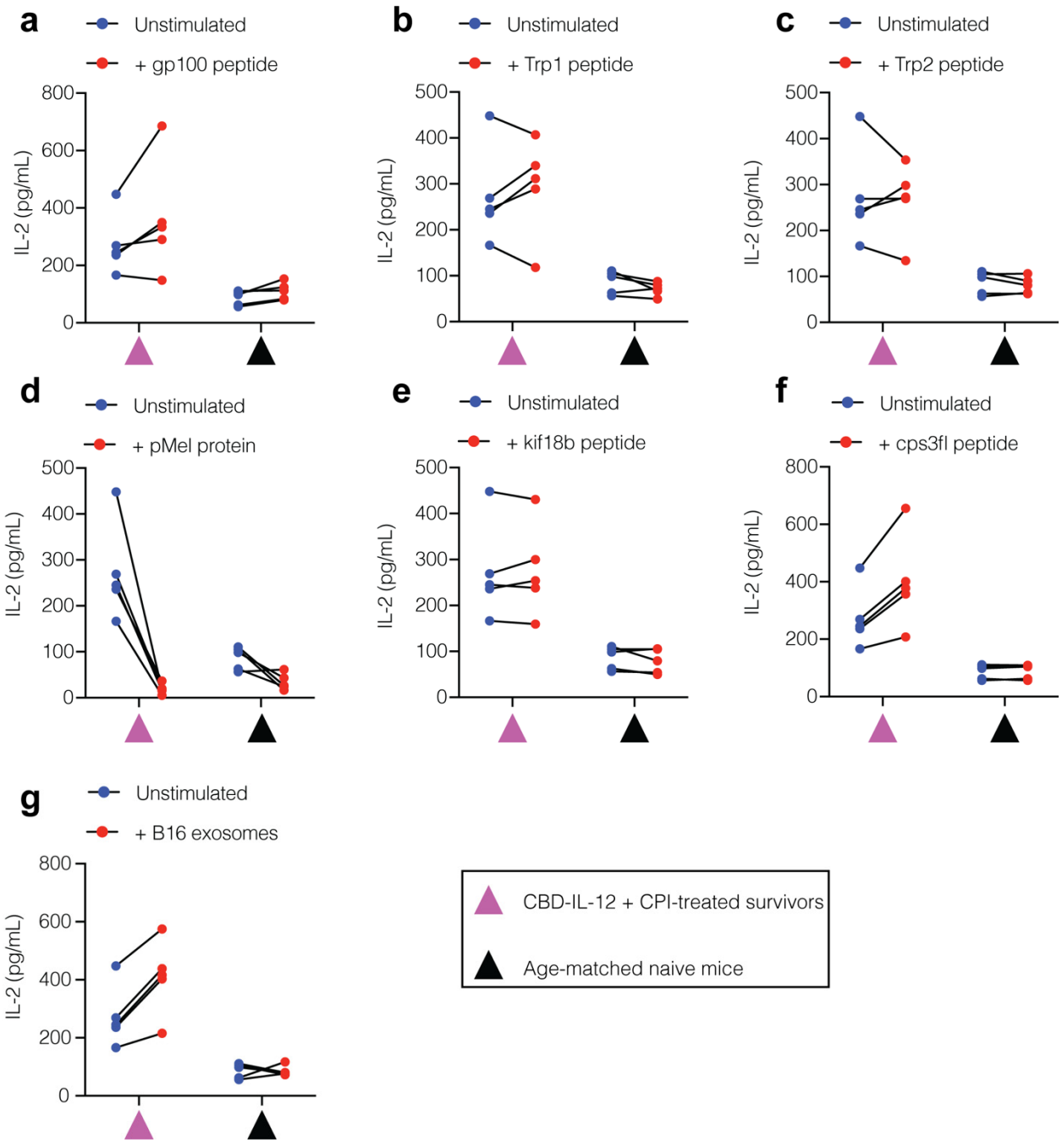

Supplementary Fig. 10 | IL-2 secretion of splenocytes from CBD-IL-12 + CPI-treated survivors and age-matched naïve mice upon antigen restimulation. a-g, Mice were treated as described in Fig. 6a,b. Spleens from surviving mice (n = 5) or age-matched naïve mice (n = 5) were harvested and stimulated with indicated antigens. IL-2 secretion from the supernatants was detected by ELISA. The differences between stimulated and unstimulated wells were used to construct the heat map shown in Fig. 6c. Experiment was performed twice, with similar results.

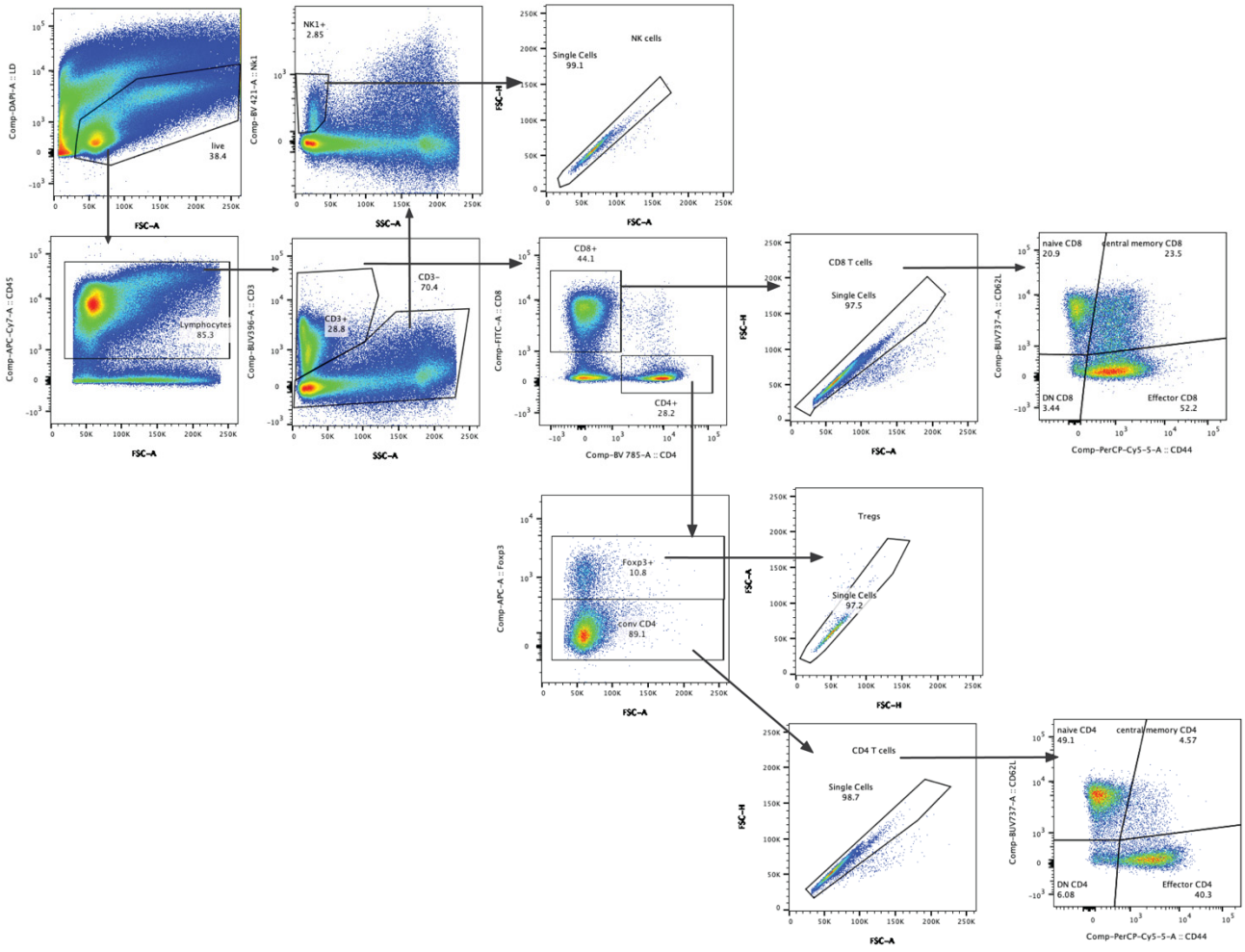

Supplementary Fig. 11 | Representative gating strategy for identifying T/NK cells in the lungs.

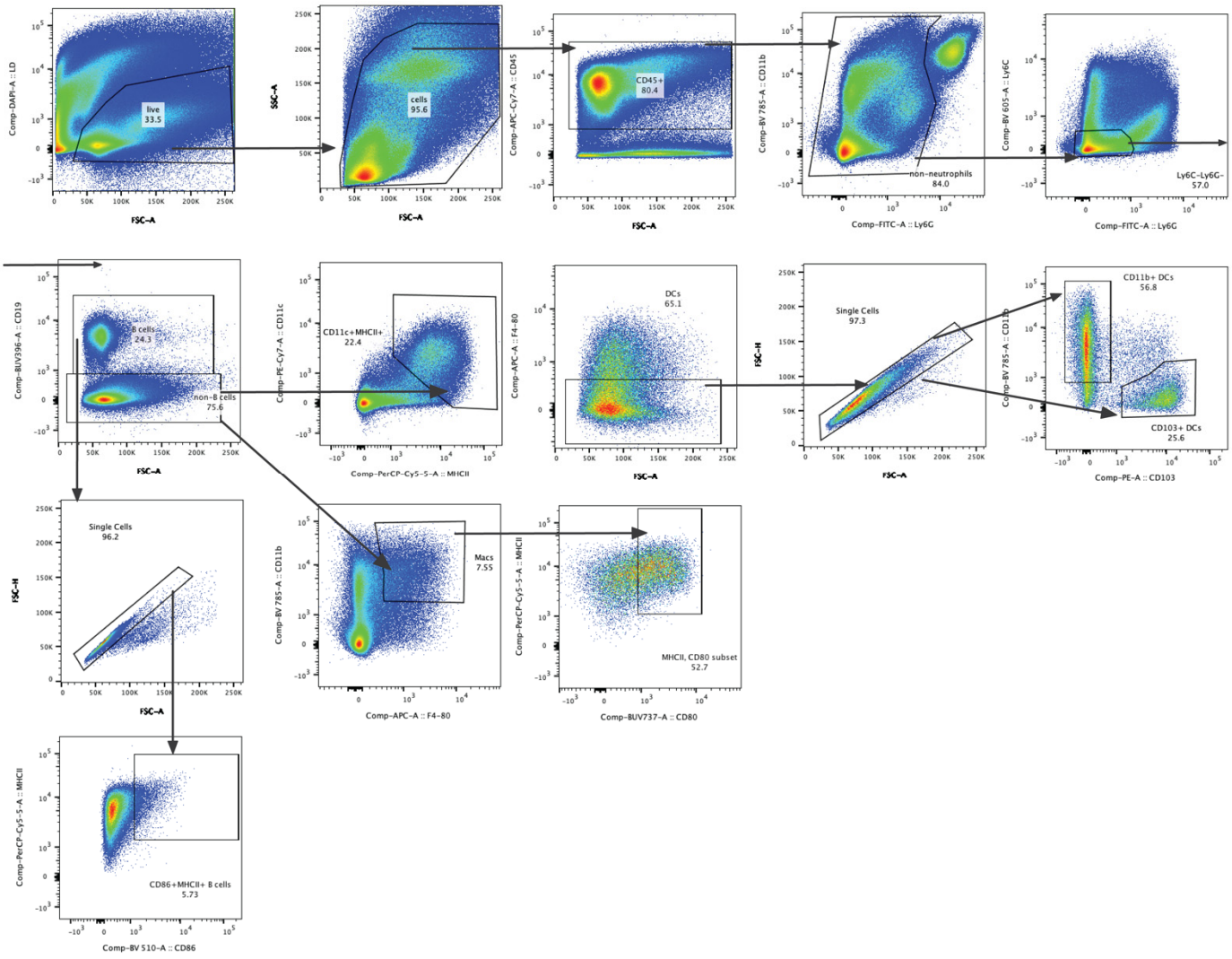

Supplementary Fig. 12 | Representative gating strategy for identifying myeloid cells in the lungs.

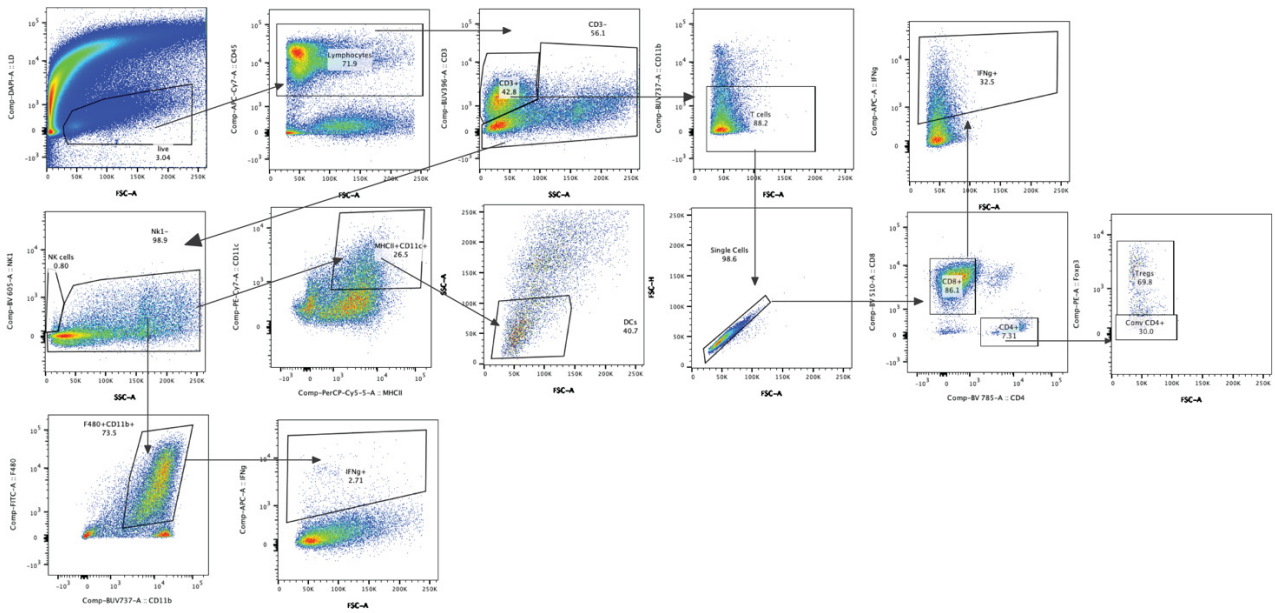

Supplementary Fig. 13 | Representative gating strategy for identifying immune cells producing IFNγ in the primary B16F10 melanoma. The same IFNγ$^+$ gate was applied to all cell populations.